

Article

# Operation and Control of a Hybrid Power Plant with the Capability of Grid Services Provision

Ayman B. Attya \* and Adam Vickers

Department of Engineering and Technology, University of Huddersfield, Huddersfield HD1 3DH, UK

\* Correspondence: a.attya@hud.ac.uk

**Abstract:** The integration of distributed power plants that rely on renewable energy sources (RESs) is a major challenge for system operators (SOs) due to the variable nature of the input energy (e.g., wind and solar irradiation) to these power sources. A key solution to such a challenge is to coordinate and combine the power generation of these sources such that their behavior is closer to a conventional and dispatchable power station, taking into account the limitations imposed by the battery storage system (BESS), so it is seen as a hybrid power plant (HPP) from the SOs' viewpoint. This paper develops a model of HPP that encompasses two generation technologies, wind and photovoltaic farms, which are assisted by a BESS. The paper proposes a comprehensive control method that can smooth the HPP output with minimized energy rejection whilst enabling the HPP to provide synthetic inertia and primary frequency response, which are grid-code compliant. The proposed control method is validated through various scenarios, which are implemented on a detailed electromechanical test system modeled in MATLAB/Simulink. The results show and quantify the achieved improvement on stabilizing the HPP capacity factor under variable wind speed. The HPP also enhances the system response to frequency events.



**Citation:** Attya, A.B.; Vickers, A. Operation and Control of a Hybrid Power Plant with the Capability of Grid Services Provision. *Energies* **2021**, *14*, 3928. <https://doi.org/10.3390/en14133928>

**Keywords:** frequency support; wind power; solar power; hybrid power plants; battery storage; control systems; power smoothing; capacity factor

Academic Editor:  
Dimitrios Katsaprakakis

Received: 31 May 2021  
Accepted: 28 June 2021  
Published: 30 June 2021

**Publisher's Note:** MDPI stays neutral with regard to jurisdictional claims in published maps and institutional affiliations.



**Copyright:** © 2021 by the authors. Licensee MDPI, Basel, Switzerland. This article is an open access article distributed under the terms and conditions of the Creative Commons Attribution (CC BY) license (<https://creativecommons.org/licenses/by/4.0/>).

## 1. Introduction

There are obvious and growing efforts worldwide to increase and expand RES contributions to the generation mix, replacing the conventional power stations that rely on fossil fuels [1]. However, SOs, technology developers and RES farms operators are still facing the fundamental challenge of maintaining power system stability subject to potential risks caused by the variable nature of RES output (except hydropower plants), which depend on meteorological conditions, e.g., wind speed, tides, solar irradiation, etc. [2].

The literature covers many aspects of the grid-friendly operation of RESs, which includes the provision of frequency support [3,4] and voltage support [5], among other types of ancillary services. Significant attention has been given to the provision of frequency support by wind turbines and wind farms (WFs), where supplementary controllers are integrated into the controls of Type 3 (double-fed induction generator) and Type 4 (full rated synchronous generator) wind turbine generators (WTGs) to be capable of providing a regulated active power increment during frequency excursions. The two most common concepts are pitch-deload and kinetic energy extraction [6]. The two concepts have been extensively implemented in the literature through different controller designs, which usually require the system frequency, WTG pitch angle and speed or available power as input signals; meanwhile, the output signal is an amended reference torque or power signal as well as reference pitch angle. It is worth noting that this paper already considers this technology in the developed HPP model, as explained in Section 2.

Voltage support by RES is another active field of research and technology developments. Many papers have proposed various control methods to enable wind turbines and

PV systems to provide reactive power compensation during voltage dips and overvoltage events. This is mainly focused on the integration of supplementary controllers into the  $d$ - $q$  currents control loops to regulate active and reactive power during faults. The challenge in this field is more limited in comparison to frequency support as there is no need to sustain certain amounts of active power for relatively long intervals. In addition, the presence of the power electronics interface, i.e., back-to-back converters, facilitates the implementation of these controls, making them very responsive and grid-compliant [7].

The combination of multiple power sources and generation technologies in one entity has received special interest from stakeholders, and they are often referred to as HPPs. They rely on a variety of power generation and energy sources, hence, the use of the word 'hybrid'. Some research also uses the term 'virtual power plants' [8]. However, this expression might not be an accurate description of the developed energy system in this paper, as all the elements should be physically available. One of the common examples of virtual power plants is WFs, which are controlled to behave as a typical synchronous generator, i.e., virtual synchronous generator; however, this is outside the paper scope.

The authors of [9] aim to validate simplified simulation models of the various energy sources that can be parts of hybrid power plants. However, they do not offer specialized control methods to provide ancillary services or improve the ability of the HPP output dispatch as seen from the SOs viewpoint. The study is also more focused on grid-forming control of WTGs in small microgrids. The authors of [10] developed sensitivity studies to exploit various energy storage technologies, where they examined lead-acid battery packs along with reversible polymer electrolyte fuel cells. They have also included a diesel generator as a backup energy source which compromises the 'green' nature of the HPP, leading to CO<sub>2</sub> emissions. The review article [11] provides a high-level comprehensive discussion on two main aspects, the optimization techniques to size the generation units forming an HPP, and the different approaches implemented to design control methods of HPPs. It is mentioned that the offered control methods in the literature can consider either economic challenges or technical challenges, and this manuscript is focused on the technical challenges related to the coordinated provision of ancillary services by the power units forming the HPP. The research presented in [12] provides an overview of the various generation technologies that can contribute to HPPs, including wind and hydro power. It also presents the advancement in probabilistic algorithms used to estimate the capacity factor of renewable energy, with some real case studies for solar power plants in the US. However, they do not discuss modeling of HPPs and the corresponding holistic controls to enable further functionalities, including ancillary services provision. This paper considers the feasibility of providing frequency support services from more than one power source, i.e., the BESS and the wind farm, while the third power source, i.e., PV farm, does not sacrifice any of its generated power to maintain a reserve margin. In addition, the proposed control utilizes the online HPP capacity factor as a key driver for the HPP's dispatchability and control of the integrated BESS.

Energy storage systems have been widely investigated in the literature as pivotal elements in the increase of RESs share in the generation mix. There are various technologies that can be used to sustain power generation and provide ancillary services; however, the most common are hydro-pumped storage (more than 98% of grid-scale energy storage worldwide) and battery energy storage [13]. Even though hydro-pumped storage is the most common, it has special geographic requirements and huge capital investments, whilst also being less responsive compared to BESS. However, BESSs are still facing a higher levelized cost of energy compared to other power-generation technologies. In addition to the essential cooling systems, which represent a major challenge for warm countries, BESSs are still a relatively expensive option.

The key roles of BESSs can be categorized into four areas: concurrent provision of grid services, e.g., frequency and voltage support [14]; optimal BESS operation under various constraints and lifetime boundaries [15]; special controls of the power electronic interface in the case of a weak grid, e.g., grid-forming controls [16]; and coordinated operation

with RES. Authors in [13] propose a control method for BESSs to provide both energy and frequency control services. In [17], the BESS is sized according to the seasonal historical generation of a WF, and then a frequency support method is proposed, which relies on a certain droop profile. The authors of [18] implemented predictive control to make the distribution feeder dispatchable within a 5 min time window considering the operational constraints of the integrated BESS.

In the light of this literature review, and to the authors' best knowledge, the operation and modeling of detailed HPPs is an active topic that requires further contributions. This paper proposes the design and control methods of a complete HPP, where the incorporated BESSs power generation/demand is managed according to the WF and PV farm (PVF) generation. The BESS has two control modes; first, it can stabilize the HPP output at a predefined capacity factor (CF), and second, provide active power support during frequency drops. The priority is always given to mode 2: frequency support, where the provided increment in active power is regulated to comply with a certain generic grid code. Moreover, and to exploit further capabilities of such HPPs, the WTGs are equipped with a supplementary frequency support control, which relies on the pitch deloading concept to provide additional security to the interconnected power system during frequency events. The support from the WF can also be seen as a backup when the state of charge (SOC) of the BESS falls below its minimum threshold; hence, the BESS will not be able to provide active power support in the case of frequency drops. The presence of the BESS should compensate both technically and economically for the wasted electrical energy due to deloading the WF at normal operation (i.e., when the frequency is within the safe deadband), where the BESS acts as a buffer absorbing excess/injecting deficit power to maintain a certain CF, fulfilling the promised power rating of the HPP. It is worth mentioning that The HPP research can be focused on either the technical and/or the economic aspects [11]. The presented study and the developed models and control methods are focused on the technical operation and coordination between the power sources forming the HPP. The sizes of the WF, PVF and the BESS are prerequisites to the proposed operation method.

The rest of the paper is organized as follows: Section 2 explains the developed BESS controls and their coordination with PVF and WF instantaneous generation. Section 3 describes the controls of the three power sources, the implemented test system, the corresponding simulation model, and the applied case studies. Section 4 presents the results obtained and the corresponding technical explanations. Finally, Section 5 provides a brief discussion that includes the main findings and conclusions.

## 2. HPP Active Power Management

The considered HPP is composed of three power sources: WF, PVF and the BESS. In this section, the control methods integrated into the BESS and WF to provide ancillary services are explained.

### 2.1. BESS Roles

The BESS has two roles, the first being to maintain the CF of the HPP within a certain predefined value, which should be decided in the planning stage of the HPP using the available meteorological data and the technical specifications of the installed power sources. In this study, the target capacity factor ( $CF_0$ ) is assumed to be 35%, which is an average value for many WFs according to the literature [19]. The CF is calculated continuously using (1), according to the fluctuations of wind and solar irradiation; hence, the generated power by the WF and PVF:

$$CF = \frac{P_{WF} + P_{PVF} \pm P_{BESS}}{P_{WF}^R + P_{PVF}^R}; +VE : \text{BESS is discharging}, -VE : \text{BESS is charging} \quad (1)$$

where  $P_{WF}$ ,  $P_{PVF}$  and  $P_{BESS}$  are the instantaneous power generation of the WF, PVF and the BESS, respectively, while  $P_{WF}^R$  and  $P_{PVF}^R$  are the rated power of the WF and the PVF, respectively. As observed, the CF excludes the BESS-rated power in the denominator, as

the function of the BESS is to sustain an almost constant output of the PVF and WF from the viewpoint of the grid operator, i.e., it acts as a buffer where it stores excess energy or compensates for lower generation compared to  $CF_0$ . Accordingly, the active reference power of the BESS in CF tracking mode ( $P_{BESS}^{CF}$ ) is calculated using (2):

$$P_{BESS}^{CF} = (CF - CF_0) \times \frac{sk_p^{CF} + k_s^{CF}}{s(sT_f + 1)} \times (P_{WF}^R + P_{PVF}^R) \times \frac{1}{P_{ref}^f} \tag{2}$$

where  $k_p^{CF}$  and  $k_i^{CF}$  are the proportional and integral gains of the PI controller responsible for setting  $P_{BESS}^{ref}$ ,  $P_{ref}^f$  is the reference power factor at which the BESS inverter is operating, i.e., assumed to be a unity power factor, and 's' is the Laplace operator.

According to (2), the BESS will be charged when  $CF > CF_0$ , where  $P_{BESS}^{ref}$  will have a positive value, and vice versa. The corresponding reference DC current of one rack in the BESS ( $I_{rack}^{ref}$ ) is calculated using (3)

$$I_{rack}^{ref} = \frac{P_{BESS}^{CF}}{N_{racks} \times V_{BESS}^{ref}} \tag{3}$$

where  $N_{racks}$  is the number of parallel racks in the BESS and  $V_{BESS}^{ref}$  is the reference DC voltage of the BESS. The polarity (i.e., sign) of  $I_{rack}^{ref}$  indicates whether the BESS is charging (positive current) or discharging (negative current).

The second key role of the BESS is to provide synthetic inertia and primary reserve. The main objective, in this case, is to regulate the change in active power provided by the BESS ( $\Delta P_{BESS}^f$ ) to suppress the frequency deviation and contribute to reducing the gap between generation and demand. The value of  $\Delta P_{BESS}^f$  is estimated through the generic frequency support control shown in Figure 1, where the numeric values of the corresponding parameters are collated in Table 1.

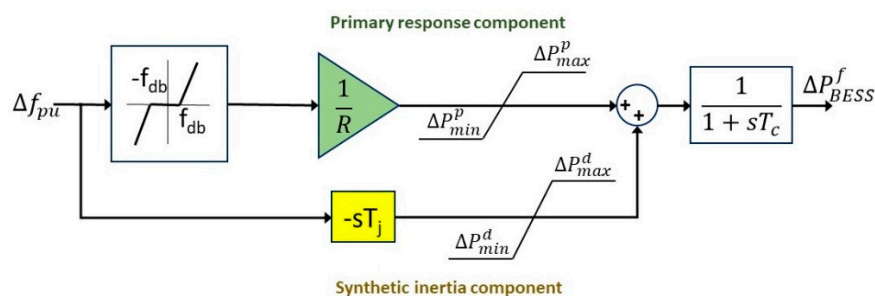


Figure 1. Frequency support controller of the BESS.

Table 1. Parameters of the frequency support controller of BESS.

Parameter	Symbol	Value
Frequency deadband	$f_{db}$	$\pm 20$ mHz
Frequency droop	R	4%
Synthetic inertia component limits	$\Delta P^d$	$\pm 0.1$ pu
Primary response component limits	$\Delta P^p$	$-0.8$ to $0.1$ pu
Inertia time constant	$T_j$	10 s
Communication time delay	$T_c$	20 ms

The coordination between the CF tracking functionality and frequency support during frequency events (i.e., the frequency is outside the safe deadband) is an additional challenge. Many proposals give priority to frequency support, which means turning off the CF tracing

functionality. However, this could be threatening for system stability in some scenarios. For example, if the BESS was operating in the discharging mode to elevate the CF of the HPP, and a frequency drop occurred, the BESS will switch quickly to frequency support mode. However, this could lead to less power injected by the BESS to the grid if compared to its original value just before the event, i.e.,  $\Delta P_{BESS}^f < P_{BESS}^{CF}$ , which will aggravate the generation–demand imbalance. Note that although the power is injected by the BESS in both operation modes, the magnitude may have a significant impact. Another scenario is when the HPP output has naturally increased during the frequency drop due to an increase in wind speed and/or solar irradiation. In such a case, maintaining the CF to its target value, which could be lower compared to the actual HPP generation, will curtail the HPP capability to arrest the frequency nadir and rate of change of frequency (RoCoF). To overcome this issue, the control logic represented by (4) and illustrated in Figure 2 is implemented,

$$\text{Support operation : } I_{rack}^{ref} = \begin{cases} \frac{\pm P_{BESS}^{CF} \pm \Delta P_{BESS}^f}{N_{racks} \times V_{BESS}^{ref}} & \text{if } \text{sign}(P_{BESS}^{CF}) = \text{sign}(\Delta P_{BESS}^f) \\ \frac{\Delta P_{BESS}^f}{N_{racks} \times V_{BESS}^{ref}} & \text{else} \end{cases} \quad (4)$$

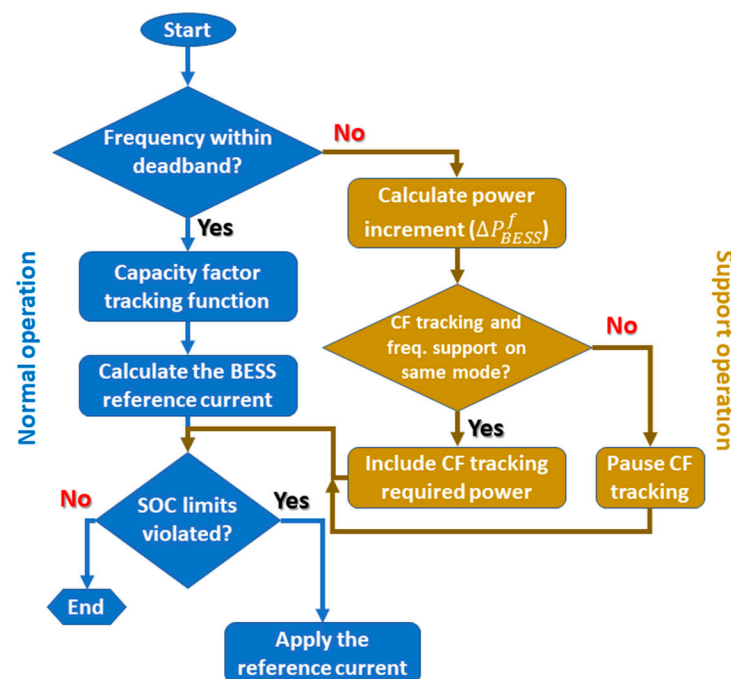


**Figure 2.** Flowchart of the proposed coordination between frequency support and CF tracking.

The reference current is evaluated such that the CF tracking functionality is allowed only when its mode (charging or discharging) is similar to the mode required by frequency support. For example, if there is a frequency spike, the BESS should be charged to absorb the additional power which is causing the imbalance. If the CF was already low during such an event, the BESS will be required to discharge to elevate the CF aiming to reach  $CF_0$ . Hence, the proposed method will pause the CF tracking facility in this scenario, as it should be more useful to retain frequency stability faster with minimised fluctuations. Therefore, the proposed control does not simply add the reference power of CF tracking as well as the frequency support controller together. This is indicated in the conditional block within the ‘Support operation’ path in Figure 2.

### 2.2. Frequency Support by WF

The applied method can be classified as delta deloading [20], where WTG output is deloaded continuously by a constant factor ( $D_F$ ) through increasing the pitch angle. The available output ( $P_{ref}^o$ ) refers to the WTG output when it follows the conventional Maximum Power Tracking (MPT). The ratio  $P_{ref} / P_{ref}^o$  in (5), which is called the adjustment factor ( $A_F$ ), is controlled using (6):

$$P_{ref} = A_F \times P_{ref}^o \tag{5}$$

$$A_F = \begin{cases} 1 - D_F, & f \geq f_{low} \\ D_F \times \left(1 - \frac{f_0 - f}{f_{drop_{max}}}\right), & (f_0 - f_{drop_{max}}) < f < f_{low} \\ 1, & f \leq (f_0 - f_{drop_{max}}) \end{cases} \tag{6}$$

where  $f_0$  and  $f$  are the nominal and actual frequencies, respectively. The active power set-point is reduced by  $D_F = 0.15$ ; meanwhile, the rotor speed is regulated to the nominal value based on the incident wind speed at normal frequency conditions. This is the normal operation mode, where  $A_F$  is less than 1. When frequency drop violates a safe margin ( $f_{low}$ ), the deloading ratio is curtailed by a droop gain until frequency drop reaches a preset threshold ( $f_{drop_{max}}$ ), at which  $A_F = 1$ . The supplementary controller shown in Figure 3 is integrated into speed and pitch control in the MATLAB benchmark of Type 4 WTG. The variability of  $A_F$  according to the incident frequency deviation with two types of deloading, i.e., droop and step, is illustrated in Figure 4. The values of the controller parameters are collated in Table 2.

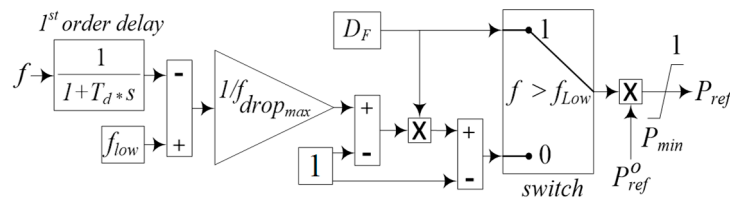


Figure 3. Block diagram of the implemented droop pitch deloading.

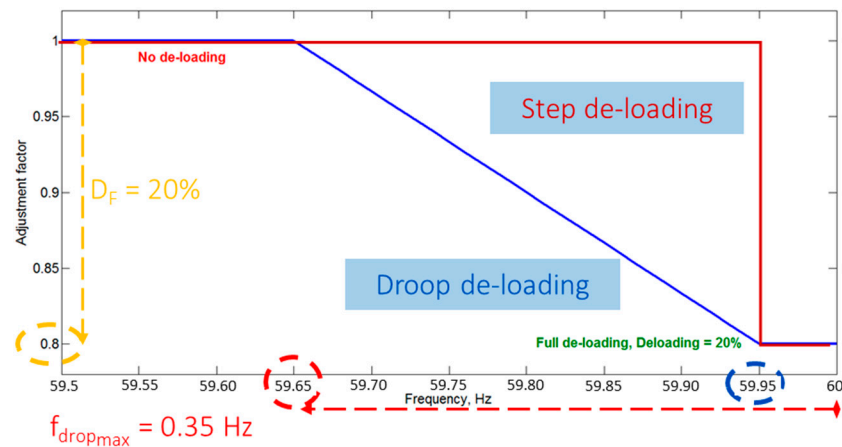


Figure 4.  $A_F$  setting according to frequency variability and method of deloading.

**Table 2.** The values of the parameters of the implemented pitch deloading control.

Parameter	Symbol	Value
Max. frequency drop	$f_{\text{drop,max}}$	0.25 Hz
Frequency threshold to initiate support	$f_{\text{low}}$	59.95 Hz
Deloading factor	$D_F$	15%
Time delay	$T_d$	10 ms

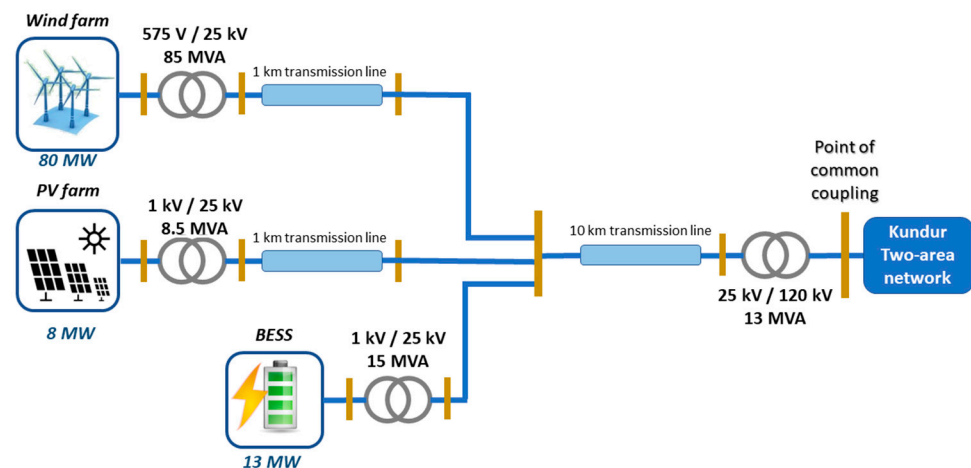
It should be highlighted that this paper focuses on the dynamic operation of the HPP, namely, the control of active power produced by the HPP as a whole either during normal frequency conditions or during frequency excursions relying on the presence of the BESS as a key element in the HPP. The proposed control method should not have an adverse negative impact on the HPP economics. In particular, the BESS lifetime might be slightly affected due to its dual role as frequency support provider as well as CF tracker; however, most of the modern BESS modules are capable of handling fast and continuous charging/discharging dynamics without a critical impact on their durability. The adjustment of  $CF_o$  can be made related to market spot price as well as grid dynamics.

### 3. Test System and Case Studies

This section explains the implemented test system to demonstrate the application of the proposed control method. It also describes the various case studies that have been designed to examine the system response under different operating conditions, during and after some system events.

#### 3.1. HPP Model and the Interconnected Network

The HPP encompasses three power sources: a WF, PV installation (PVF) and a BESS, as illustrated in Figure 5. Every WTG inside the WF, as well as the PV installation, is coupled to the network through a power electronics interface.

**Figure 5.** Single line diagram of the HPP and its connection to power network.

##### 3.1.1. The Wind Farm

The WF is modeled as an aggregate WTG, which includes the turbine, drive train, synchronous generator and full-rated back-to-back converter models as well as their controllers. The mathematical modeling and explanation of Type 4 WTG has been vastly investigated in the literature [21]. The WTG controls are amended, as explained earlier in Section 2, to integrate the pitch-deload frequency support controller. The harnessed wind power ( $P_w$ ) is calculated using the well-known Equations (7)–(9):

$$P_w = 0.5 \cdot \rho \cdot C_p \cdot A \cdot v_w^3 \quad (7)$$

$$C_p(\lambda, \beta) = 0.22 \cdot \left( \frac{116}{\lambda_i} - 0.4\beta - 5 \right) \cdot e^{-\frac{12.5}{\lambda_i}} \quad (8)$$

$$\lambda_i = \frac{1}{\frac{1}{\lambda + 0.08\beta} - \frac{0.035}{\beta^3 + 1}} \quad (9)$$

where  $C_p$  is the performance coefficient,  $\lambda$  is the tip speed ratio and both are dimensionless.  $\beta$  is the pitch angle in degrees,  $A$  is the rotor swept area in  $\text{m}^2$  and  $\rho$  is the air density in  $\text{kg}/\text{m}^3$ . The WTGs apply the conventional maximum power tracking (MPT) approach, which relies on adjusting the rotor speed through a tracking function based on the output power of the WTG ( $P_{WTG}^{out}$ ) in per unit of the WTG rated power, as in Equation (10).

$$\omega_{ref} = -0.555 \cdot (P_{WTG}^{out})^2 + 1.183 \cdot P_{WTG}^{out} + 0.425 \quad (10)$$

The deviation between the optimum reference rotor speed and the actual speed is fed into the duty cycle controller of the machine side converter, as illustrated in Figure 6. Further explanations of the WTG benchmark can be found in MATLAB documentation. The rated power of the WF is 80 MW, i.e.,  $40 \times 2$  MW Type 4 WTGs.

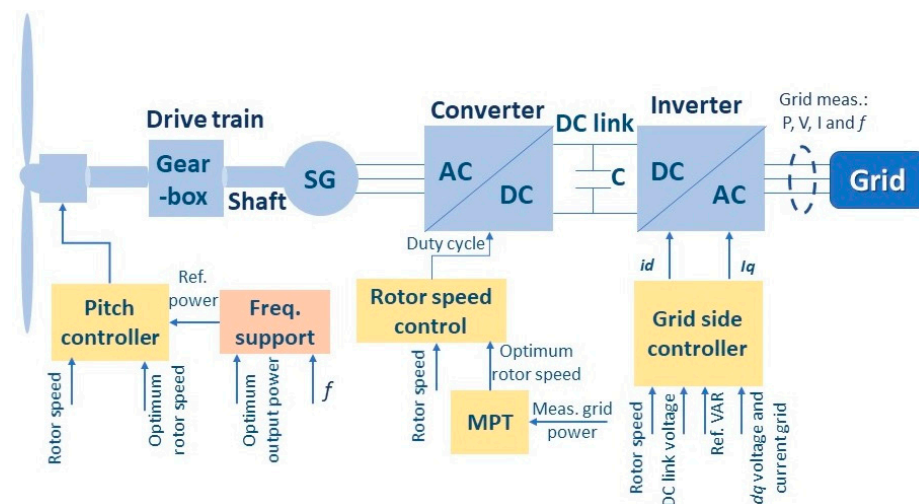


Figure 6. Schematic of the implemented Type 4 WTG and the associated controls.

### 3.1.2. The PV Farm

The PVF is modeled as an aggregation of 20 groups, each of 400 kW rated power, where the combined power of the farm is 8 MW at 1-Sun. Each group is formed of 128 parallel strings; each string includes 20 series modules. The PV modules are controlled using the conventional Perturb and Observe control approach to adjust the modules currents, achieving maximum power tracking according to the incident solar irradiation [22]. The PVF is connected to the grid via a DC boost converter that regulates the DC link voltage, then an inverter to convert the DC power into AC power, which is fed into the grid. The temperature is kept constant at an average value of 30 °C.

### 3.1.3. The Battery Storage System

The MATLAB benchmark model of the Li-Ion cell is the fundamental component of the BESS, whose design is inspired by the commercial BESS in [23]. The BESSs' power size was estimated upon the average output power of the WF, where the applied variable wind speed is considered as a reference. The BESS power capacity is assumed to be 15% of the HPP-rated power, i.e., WF plus PVF rated power. The BESS reference value of the total charging/discharging current is calculated using the controller, explained in Section 2. The main characteristics of the three power sources are summarized in Table 3. The common technical characteristics of the four identical synchronous power plants are in Table 4.

**Table 3.** Main parameters are ratings of the WF, PVF and the BESS.

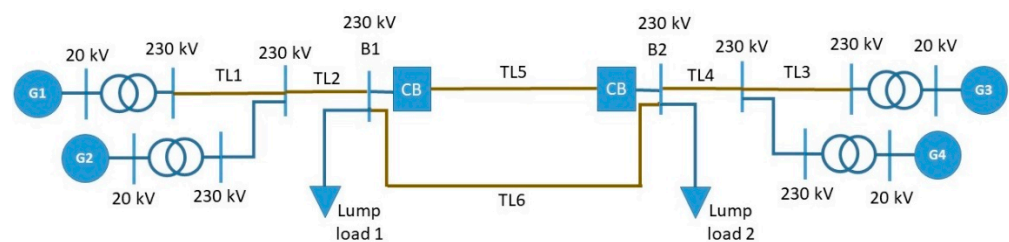
Parameter	Wind Farm	PV Farm	BESS
Rated power [MW]	80	8	13
Technology	Type 4	Monocrystalline PERC	Li-Ion
Units no. and structure	40 × 2 MW WTGs	256 strings × 5 modules	10 cells × 28 modules × 46 racks
Control method	MPT—Power speed control and pitch deloading	MPT—Perturb and Observe	Two modes: CF tracking and frequency support

**Table 4.** The values of the parameters of the synchronous power plant.

Parameter	Value	Parameter	Value
Rated voltage	20 kV	PSS Time constant	15 ms
Inertia	6.2 s	PSS gain	30
Governor droop	5%	PSS washout constant	10 s
Exciter gain	200	Output limits	±0.15 pu

### 3.1.4. The Interconnected Network

The implemented two-area benchmark was modified to reduce the conventional generation capacity, i.e., the combined ratings of the generators 1 to 4, i.e., G1 to G4, as illustrated in Figure 7. Hence, the loads in the two areas are also scaled down to match the total generation capacity of the grid. The total synchronous generation is 1440 MVA, and they are loaded by about 85% to feed the connected loads. This should be considered as a challenging scenario of a weak grid. Further details about the two-area model are available in [24] and MATLAB documentation.

**Figure 7.** Single line diagram of the two-area Kundur network.

### 3.2. Case Studies

The variable wind speed and solar irradiation profiles which are implemented in all case studies is shown in Figures 8 and 9 respectively. This is realistic wind speed data represent a typical wind speed profile. The applied simulation time span is relevant to the nature of the study and the objectives of the control method, which are focused on active power control and its impact on frequency dynamics. The presented study applies randomly changing insolation within the range of 700–1000 W/m<sup>2</sup> to reflect realistic and moderate variations at average weather conditions.

Case study 1 (base case)—A sudden increase in load with 88 MW occurs in Area 1 at  $t = 8$  s. All the special controls are OFF, including the CF tracking. This should be the base case, which is used as a reference to observe the impact of various scenarios and control methods on both the power source dynamics as well as the system response.

Case study 2—variable wind/gull support: both the WF frequency support and the BESS functionalities (CF tracking and frequency support are ON). The system is subject to the same load event of Case study 1.

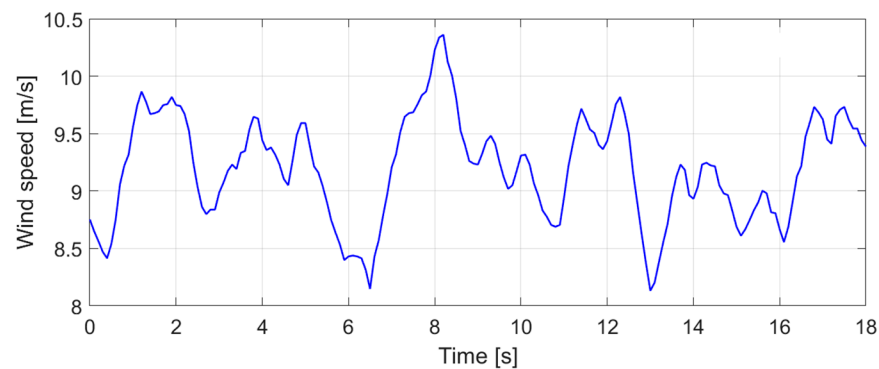


**Figure 8.** The variable wind speed profile applied in Case studies 1, 2 and 3.

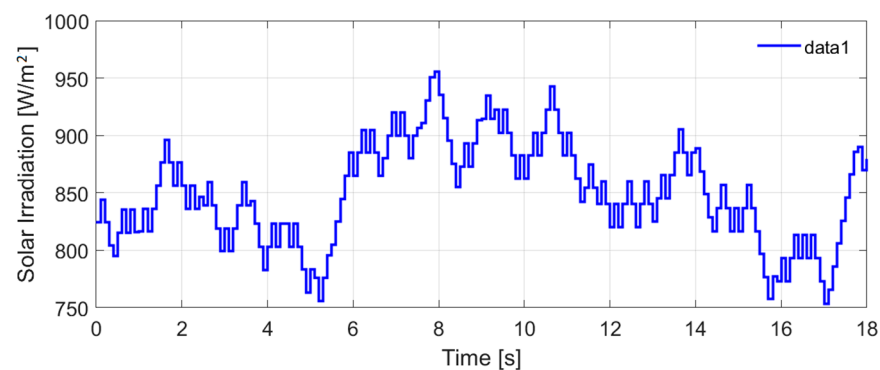


**Figure 9.** The variable solar irradiation applied in all case studies 1, 2 and 3.

Case study 3—variable wind/WF support OFF: similar to Case study 2, but the frequency support by WF is turned OFF, i.e., no deloading.

Case study 4—constant wind/no support: this is a second base case but at a constant wind speed of 9.4 m/s applying the same load event of Case 1.

Case study 5—constant wind/full support: similar to Case study 2, full support from both WF and the BESS, but at a constant wind speed of 9.4 m/s.

The constant wind speed in Case studies 4 and 5 was selected to this value as an average of the variable wind speed profile applied in the first three case studies.

#### 4. Results

The results of the five case studies are thoroughly discussed where some reflective signals are discussed separately in this section; meanwhile, the combined observations are explained in the next section. All cases are always compared to Case study 2, as it represents a realistic scenario of variable wind speed with a reasonable average; meanwhile, the other cases mainly reveal and separate the various effects of the implemented controls. The BESS cell reference current is displayed in Figure 10, where the current is maintained at zero before the CF tracking is activated at  $t = 1$  s, where the current increases in the positive direction, i.e., BESS charging, to reduce the CF until it reaches the target value at normal operation. This is clear in both Cases 3 and 5; however, in the case of constant wind speed, the current is almost constant according to the constant nature of the WF output. On the other hand, the current fluctuates in Case studies 2 and 3, following the continuous variations in WF output due to the variable wind speed. The BESS current is always higher in Case study 3 compared to Case 2, where the WF output is not deloaded in Case study 3 (frequency support is off; hence, pitch deloading is deactivated during normal operation). The conventional generation of both the WF and PVF are displayed in Figure 11 to provide a wider picture of the generation mix during the simulation time span. It can also be observed that under the given wind and solar irradiation conditions, the PVF contribution into the HPP generation mix is about 20%; meanwhile, its installed capacity compared to

the WF capacity is 10%. This also reflects the capability of the proposed control method to track  $CF_o$  using the integrated BESS, with the presence of two green power sources, which rely on two different types of input energy (i.e., solar irradiation and wind).

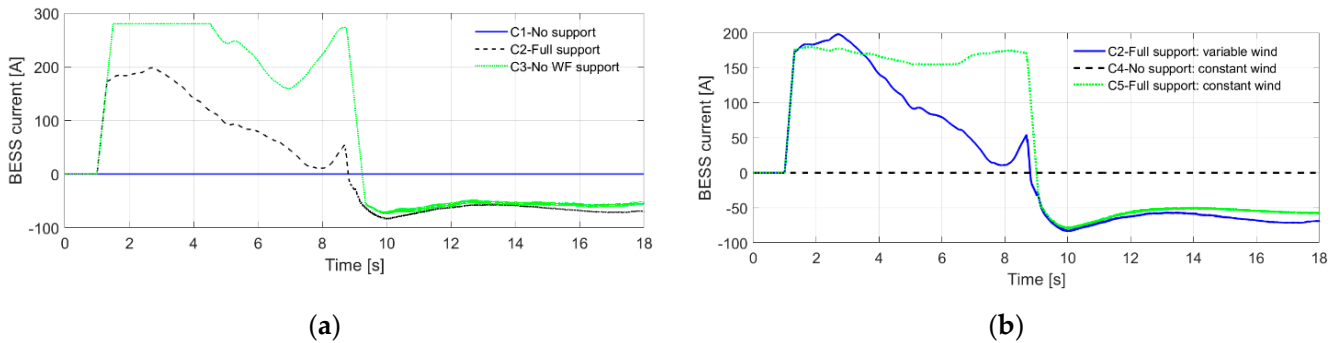


**Figure 10.** BESS cell current: (a) Variable wind speed; (b) Constant wind speed compared to Case 2.

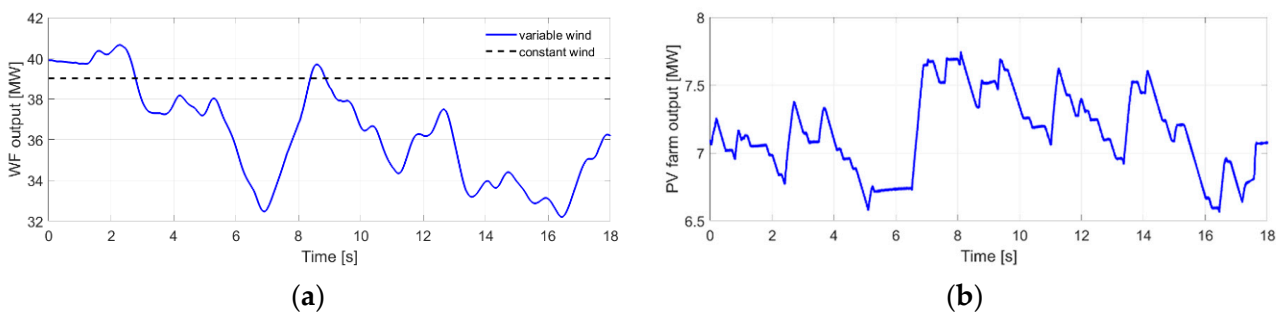


**Figure 11.** Output power: (a) wind farm under conventional operation; (b) PV farm under conventional operation.

The higher WF output in Case study 3 requires the BESS to charge more, keeping the CF within the targeted value. At  $t = 9$  s, the frequency events occur; hence, the BESS should respond in an opposite way to the cause of the frequency event. In this case, there is a frequency drop caused by a sudden increase in load; hence, more active power should promptly be injected into the power system. Since the BESS was in charging mode just before the event, it has to switch discharging mode, i.e., negative current, to comply with the frequency support requirements, as explained earlier in Section 2. Similar outcomes are deduced based on the in/output power of the BESS shown in Figure 12.

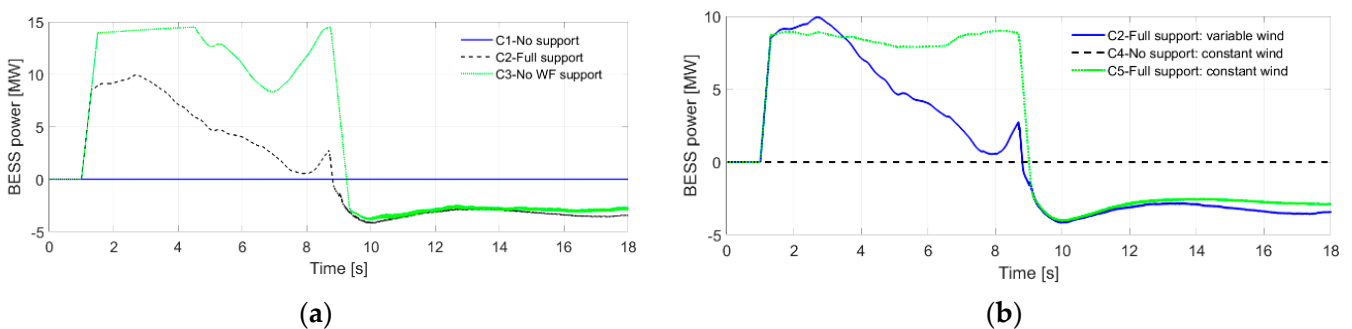


**Figure 12.** BESS total power: (a) variable wind speed; (b) constant wind speed compared to Case 2.

The successful operation of the CF tracking functionality is demonstrated through the behavior of the CF displayed in Figure 13, where the CF drops to the target value within a very short time from CF tracking activation. The designed PI control and the selected input signal enabled such a smooth and fast tracking in spite of the variable nature of wind speed at 1 s time resolution. At constant wind speed in Figure 13b, the CF maintained an almost

flat line because of the constant wind speed; however, once the frequency excursion occurs, the CF increases rapidly as the HPP injects more active power to arrest the frequency nadir and mitigate the consequences of the sudden increase in load. The impact of WF deloading can also be seen on the CF, which has some slight fluctuations in Case study 3 compared to Case study 2.

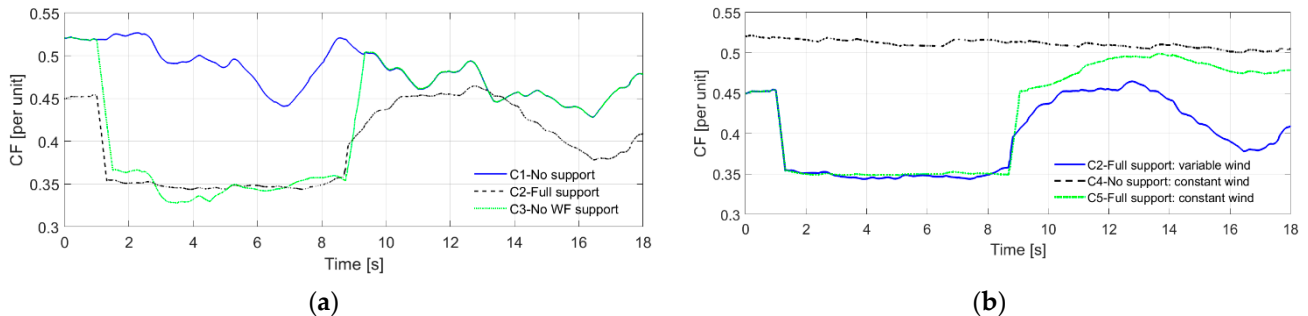


**Figure 13.** Capacity factor: (a) variable wind speed; (b) constant wind speed compared to Case 2.

The system frequency shows an expected behavior in the examined case studies as in Figure 14, where the frequency drops very slightly once the CF tracking is activated at  $t = 1$  s; however, the frequency deviation is still within the safe margin, which is  $\pm 0.05$  Hz in this research work. The frequency is less than the nominal value on this occasion, as the BESS will activate the charging mode to reduce the CF to the target value.

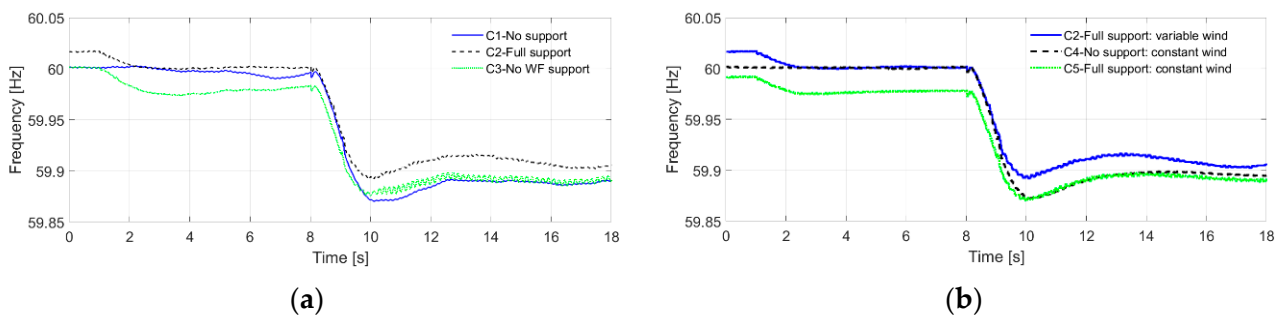


**Figure 14.** System frequency measured at the HPP point of connection: (a) variable wind speed; (b) constant wind speed compared to Case 2.

The contribution of HPP to frequency support during the event does not clearly impact either the RoCoF or the worst frequency deviation, i.e., nadir, due to the limited HPP capacity compared to the aggregate capacity of the four synchronous generators, as they dominate the generation mix. There was no clear impact of wind speed variability due to the domination of conventional generation mix as well as the activation of CF tracking, which maintained an almost constant HPP output, as discussed previously. It is worth mentioning that the authors will investigate further scenarios and implement the proposed methods and model of the HPP with a larger capacity which achieves higher penetration into the generation mix in their future research.

The WTG pitch angle dynamics reflect the influence of the output deloading where the pitch is always higher than zero in Case 2 of full support in Figure 15a, where its value is changing continuously according to the incident wind speed. The pitch angle is almost constant in Case 5 with constant wind speed (Figure 15b), then it drops quickly to almost zero at the frequency event following the controller response, which is explained in Section 2.2.

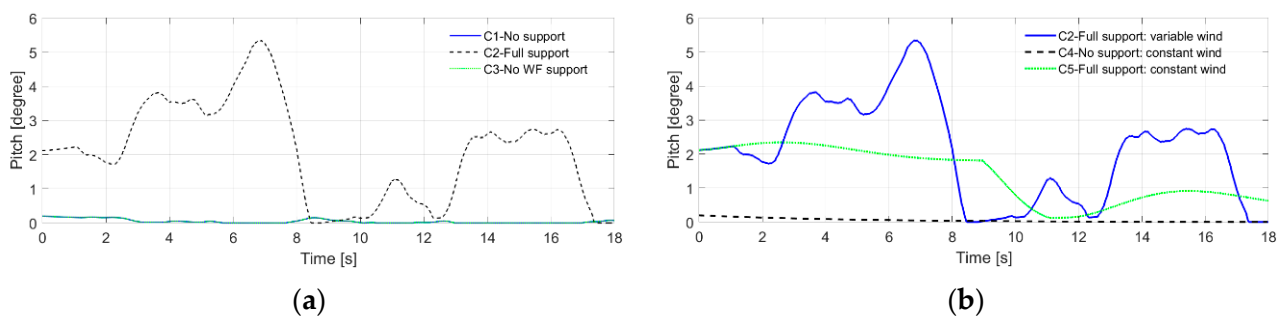


Figure 15. Pitch angle: (a) variable wind speed; (b) constant wind speed compared to Case 2.

## 5. Discussion

The proposed active power control of the HPP power sources considered two main functions: improving the ability of HPP output dispatch, i.e., keeping a constant and pre-determined CF as possible using the BESS as a buffer and the provision of synthetic inertia and primary response using the BESS as a sustainable power reserve. The implemented test system and case studies prove the successful application of the proposed control method. The BESS charging/discharging strategy provides a reasonable balance between the mitigation of uncertainty of HPP power output and the capability of frequency support. This includes the capability of CF tracking if it requires the same operation mode which is necessary for frequency support, not just to simply switch between the two functionalities simultaneously. The incorporation of a second reserve, which is the margin between the optimum and deloaded output of the WF, should reduce the stress on the BESS; however, it can reduce the HPP revenue due to the unsold amounts of energy. The included low-pass filter in the CF tracking control should also reduce the minor negative influence of continuous fluctuation in cell current. In addition, the nature of wind speed fluctuations should also suppress this influence, as the wind speed is always fluctuating around a certain average, which does not change steeply within very short intervals, similar to the profile applied in the presented case studies. Hence, the cell current does not change its direction (charging/discharging).

The size of the BESS, i.e., power rating and energy capacity, can be accurately calculated using probabilistic or deterministic methods offered in the literature. In particular, the HPP research is usually focused on either the technical and/or the economic aspects [11]. The presented study and the developed models and control methods are focused on the technical operation and coordination between the power sources forming the HPP. Therefore, the presented research considers the capacities of the wind farm, the PV farm and the BESS as prerequisites to the proposed operation methods. The sizing optimization can be developed to consider the best sharing of the HPP primary reserve between the contributions of the BESS and the WF deloaded output.

**Author Contributions:** A.B.A.: model development, writing and review. A.V.: model development and manuscript revision. Both authors have read and agreed to the published version of the manuscript.

**Funding:** This research has not received funding.

**Institutional Review Board Statement:** Not applicable.

**Informed Consent Statement:** Not applicable.

**Data Availability Statement:** Not applicable.

**Conflicts of Interest:** The authors declare no conflict of interest.

## Abbreviations

BESS	Battery Energy Storage System
CF	Capacity Factor
HPP	Hybrid Power Plant
MPT	Maximum Power Tracking
PVF	Photovoltaic Farm
RES	Renewable Energy Source
RoCoF	Rate of Change of Frequency
SO	System Operators
SOC	State of Charge
Type 3	Double-fed Induction Generators
Type 4	Full Rated Synchronous Generator
WF	Wind Farm
WTG	Wind Turbine Generators

## Symbols

$A$	Rotor swept area ( $m^2$ )
$A_F$	Adjustment factor (-)
CF	Target capacity factor (-)
$C_p$	Performance coefficient (-)
$D_F$	Deloading factor (-)
$I_{rack}^{ref}$	Reference DC current of one rack of BESS (A)
$k_p^{CF}$	Proportional gain of PI Controller (-)
$k_I^{CF}$	Integral gain of PI Controller (-)
$f$	Actual frequency (Hz)
$f_{db}$	Frequency deadband (Hz)
$f_{low}$	Frequency threshold to initiate wind power support (Hz)
$f_o$	Nominal frequency (Hz)
$N_{racks}$	Number of parallel racks in BESS (-)
$P_{BESS}$	Instantaneous generation of BESS (W)
$p_{ref}^f$	Reference power factor of the BESS (-)
$P_{WF}$	Instantaneous generation of wind farm (W)
$P_{ref}^o$	Maximum available power output of the wind farm (W)
$P_{WTG}^{out}$	Output power of the wind turbine generator (W)
$P_{PVF}$	Instantaneous generation of PV farm (W)
$P_{BESS}$	Instantaneous generation of BESS (W)
$P_{WF}^R$	Rated power of the wind farm (W)
$P_{PVF}^R$	Rated power of the PV farm (W)
$P_{BESS}^{CF}$	Reference active power of the BESS in capacity-factor-tracking mode (W)
$R$	Frequency droop (-)
$V_{BESS}^{ref}$	Reference DC voltage of BESS (V)
$\Delta P_{BESS}^f$	Change in active power provided by the BESS (W)
$\Delta P^d$	Synthetic inertia component power limit (per unit)
$\Delta P^p$	Primary response component power limit (per unit)
$T_j$	Inertia time constant (s)
$T_c$	Communication time delay (s)
$\lambda$	Tip speed ratio (-)
$\beta$	Pitch angle (degree)
$\Delta P^d$	Synthetic inertia component power limit (per unit)

## References

1. European Network of Transmission System Operators for Electricity (ENTSO-e). *Research, Innovation and Development Roadmap 2017–2026*; European Network of Transmission System Operators for Electricity (ENTSO-e): Brussels, Belgium, 2017; Available online: [riroadmap.entsoe.eu/wp-content/uploads/2016/.../entsoe\\_ri\\_roadmap\\_2017-2026.pdf](https://riroadmap.entsoe.eu/wp-content/uploads/2016/.../entsoe_ri_roadmap_2017-2026.pdf) (accessed on 1 March 2021).
2. Ackermann, T.; Martensen, N.; Brown, T.; Schierhorn, P.P.; Boshell, F.G.; Ayuso, M. Scaling up variable renewable power: The role of grid codes. *World Future Energy* **2016**. Available online: <https://www.irena.org/publications/2016/May/Scaling-up-Variable-Renewable-Power-The-Role-of-Grid-Codes> (accessed on 1 March 2021).
3. Attya, A.; Dominguez-Garcia, J.; Anaya-Lara, O. A review on frequency support provision by wind power plants: Current and future challenges. *Renew. Sustain. Energy Rev.* **2018**, *81*, 2071–2087. [[CrossRef](#)]
4. ENTSO-E WGAS. *Survey on Ancillary Services Procurement, Balancing Market Design*; Brussels, Belgium, 2018. Available online: [https://www.entsoe.eu/Documents/Publications/.../ENTSO-E\\_AS\\_survey\\_2017.pdf](https://www.entsoe.eu/Documents/Publications/.../ENTSO-E_AS_survey_2017.pdf) (accessed on 1 March 2021).
5. Hirase, Y.; Abe, K.; Sugimoto, K.; Sakimoto, K.; Bevrani, H.; Ise, T. A novel control approach for virtual synchronous generators to suppress frequency and voltage fluctuations in microgrids. *Appl. Energy* **2018**, *210*, 699–710. [[CrossRef](#)]
6. Attya, A.B.T.; Dominguez-Garcia, J.L. Insights on the Provision of Frequency Support by Wind Power and the Impact on Energy Systems. *IEEE Trans. Sustain. Energy* **2017**, *9*, 719–728. [[CrossRef](#)]
7. Wu, Y.K.; Chang, S.M.; Mandal, P. Grid-connected wind power plants: A survey on the integration requirements in modern grid codes. *IEEE Trans. Ind. Appl.* **2019**, *55*, 5584–5593. [[CrossRef](#)]
8. Pradhan, C.; Bhende, C.N.; Samanta, A.K. Adaptive virtual inertia-based frequency regulation in wind power systems. *Renew. Energy* **2018**, *115*, 558–574. [[CrossRef](#)]
9. Petersen, L.; Iov, F.; Tarnowski, G.C.; Gevorgian, V.; Koralewicz, P.; Stroe, D.-I. Validating Performance Models for Hybrid Power Plant Control Assessment. *Energies* **2019**, *12*, 4330. [[CrossRef](#)]
10. Tribioli, L.; Cozzolino, R.; Evangelisti, L.; Bella, G. Energy Management of an Off-Grid Hybrid Power Plant with Multiple Energy Storage Systems. *Energies* **2016**, *9*, 661. [[CrossRef](#)]
11. Ammari, C.; Belatrache, D.; Touhami, B.; Makhoulfi, S. Sizing, optimization, control and energy management of hybrid renewable energy system—A review. *Energy Built Environ.* **2021**. [[CrossRef](#)]
12. Dykes, K.; King, J.; DiOrio, N.; King, R.; Gevorgian, V.; Corbus, D.; Blair, N.; Anderson, K.; Stark, G.; Turchi, C.; et al. *Opportunities for Research and Development of Hybrid Power Plants*; National Renewable Energy Laboratory: Golden, CO, USA, 2020. Available online: <https://www.nrel.gov/docs/fy20osti/75026.pdf> (accessed on 22 June 2021).
13. Muruganatham, B.; Gnanadass, R.; Padhy, N. Challenges with renewable energy sources and storage in practical distribution systems. *Renew. Sustain. Energy Rev.* **2017**, *73*, 125–134. [[CrossRef](#)]
14. Namor, E.; Sossan, F.; Cherkaoui, R.; Paolone, M. Control of Battery Storage Systems for the Simultaneous Provision of Multiple Services. *IEEE Trans. Smart Grid* **2019**, *10*, 2799–2808. [[CrossRef](#)]
15. Li, T.; Dong, M. Residential Energy Storage Management with Bidirectional Energy Control. *IEEE Trans. Smart Grid* **2018**, *10*, 3596–3611. [[CrossRef](#)]
16. Jia, J.; Yang, G.; Nielsen, A.H. A review on grid-connected converter control for short-circuit power provision under grid unbalanced faults. *IEEE Trans. Power Deliv.* **2017**, *33*, 649–661. [[CrossRef](#)]
17. Attya, A.B. Integrating battery banks to wind farms for frequency support provision—capacity sizing and support algorithms. *J. Renew. Sustain. Energy* **2015**, *7*, 53125. [[CrossRef](#)]
18. Sossan, F.; Namor, E.; Cherkaoui, R.; Paolone, M. Achieving the dispatchability of distribution feeders through prosumers data driven forecasting and model predictive control of electrochemical storage. *IEEE Trans. Sustain. Energy* **2016**, *7*, 1762–1777. [[CrossRef](#)]
19. Huang, S.-J.; Wan, H.-H. Enhancement of Matching Turbine Generators with Wind Regime Using Capacity Factor Curves Strategy. *IEEE Trans. Energy Convers.* **2009**, *24*, 551–553. [[CrossRef](#)]
20. Margaris, I.D.; Papanthassiou, S.A.; Hatzigargyriou, N.D.; Hansen, A.D.; Sørensen, P.E. Frequency Control in Autonomous Power Systems with High Wind Power Penetration. *IEEE Trans. Sustain. Energy* **2012**, *3*, 189–199. [[CrossRef](#)]
21. Melício, R.; Mendes, V.M.F.; Catalão, J.P.S. Wind Turbines with Permanent Magnet Synchronous Generator and Full-Power Converters: Modelling, Control and Simulation. In *Wind Turbines*; 2011; pp. 465–470. Available online: <https://www.intechopen.com/books/wind-turbines/wind-turbines-with-permanent-magnet-synchronous-generator-and-full-power-converters-modelling-control> (accessed on 1 March 2021).
22. Ahmed, J.; Salam, Z. An improved perturb and observe (P&O) maximum power point tracking (MPPT) algorithm for higher efficiency. *Appl. Energy* **2015**, *150*, 97–108.
23. FREQCON. BESS FQ Flexible Energy Storage System. Available online: <https://www.freqcon.com/products/grid-storage/battery-energy-storage-systems-freqcon-bess-fq/> (accessed on 1 March 2021).
24. Kundur, P. *Power System Stability and Control*; McGraw-Hill Inc.: New York, NY, USA, 1994.